Operating Area Analysis of Direct and Geared Brushless-DC Motor Drives for Electric Bicycles

Ewgenij Starschich
Fakultät für Elektrotechnik und Informationstechnik
RWTH Aachen, Aachen, Germany
ewgenij.starchisch@rwth-aachen.de

Annette Muetze
Dept. of Electrical and Computer Engineering
University of Wisconsin–Madison, Madison, WI 53706 USA
and University of Warwick, a.muetze@warwick.ac.uk

***Abstract*— We use different measured bicycle riding profiles to determine the steady-state and the dynamic operating area requirements of electric bicycles. We use these data to discuss techniques to investigate the technical performance of direct and of geared brushless-dc motor drives for such applications, including efficiency-maps and -contours. Both sides of the gear are considered. The analysis shows the large influence of the control-method on the drive operating area and the reduction of the drive operating area but at a higher drive efficiency with higher gear ratios.**

***Index Terms*— Power-assisted bicycle, geared drive, efficiency, modeling, performance evaluation.**

I. Introduction

The market for electric motor powered bicycles has been growing fast during the last years. Such bicycles can be used for a large variety of purposes (e.g. [1]–[8]). Common issues such as high cost and weight can be addressed by custom-designed bicycles for given contexts [8]. Drives for electric bicycles are required to produce a variety of different pairs of torque and speed, and of rate of change of torque at a given speed. Such requirements can be analyzed using operating area maps.

In this paper, we determine the steady-state and the dynamic operating area requirements for electric bicycles from a set of measured riding profiles. These profiles had been obtained through real road tests and include different drive scenarios and riders. The requirements are compared to the performances of different direct and geared brushless-dc (BLDC) drives. To this aim, models of such drives have been implemented into the commercially available software package MATLAB® Simulink®. We discuss techniques for such analysis, considering both sides of the gear. We are not aware that such analysis has been reported so far. The work shall contribute towards identification and removal of barriers towards larger penetration of electric bicycles.

We begin the paper with some comments on the electric bicycle market to illustrate the background of our investigations (Section II) and on the motivation for such operating area analysis (Section III). Then, we determine the requirements on the steady-state and dynamic operating areas from the riding profiles obtained from real road tests (Sections IV – VI) and discuss the model implementation (Section VII). Next, we present the results for the steady-state and dynamic operating areas of different direct and geared drives with different control strategies and motors and compare them to the previously determined requirements (Sections VIII and IX). At the end, conclusions are drawn (Section X).

II. Comments on The Electric Bicycle Market

This brief overview has been given in a previous paper [9], but we repeat it here to illustrate the background of our analysis. – The market for electric bicycles and pedelecs (bicycles which only add electrical power to the power produced by the rider, but cannot fully drive the bicycle) has grown very fast during the last years. Notably in China, the spread of electric bicycles and electric bicycle manufacturing companies is very high. On the European and Japanese markets, it is smaller than in China but higher than in the US or in any other market. When compared to the Chinese market, more advanced technology is used on the European and Japanese markets, because the customers are more interested in high-quality and "high-tech" bicycles and are also able (and willing) to spend more money on the product.

Most DC-motor drives for electric bicycles offered on the US market are direct drives. When compared with a geared drive, a direct drive is simpler and less costly, but the motor is larger (and thus heavier) to produce the required torque. Most drives with BLDC-motors include a gear.

Until several years ago, the electric bicycle and pedelecs market was dominated by mostly relatively small companies specialized in this technology. Today, many larger bicycle companies, such as Trek, Giant, Gazelle, Sparta, and Sachs, have included electric bicycles and especially pedelecs into their program. The electrical part of the bicycle, including the motor, controller, and the battery system, are not developed by the bicycle manufacturer itself but are bought from companies who have specialized in these products [10]–[13].

Concerning the battery technology, there is also a difference between the European and the Chinese market. On the Chinese market, lead-acid batteries are widely used because of their relatively low cost. On the European market, lead-acid batteries are not used by any of the larger companies, but Nickel Cadmium (NiCd), Lithium Ion (Li-Ion), and Nickel Metal Hydride (NiMh) batteries [13].

III. Motivation for Operating Area Analysis

Drives for electric traction applications, and thus those for electric bicycles, have to be able to produce very many different pairs of (1) torque, T_e, and speed, ω_m, and (2) torque-slope, $\frac{T_\mathrm{e}}{dt}$, and speed. The requirements of both characteristics have to be met to ensure that a drive is performing well for the intended purpose. Fully simulating the performance of a given drive for a given riding profile in the time-domain can be very time-consuming. Yet, when designing drives, one of the first

0197-2618/07/$25.00 © 2007 IEEE

questions to be answered often is to which extent a certain drive configuration can produce the torque-speed profile of a given riding profile. If we only seek to answer this question, we can replace time-consuming individual simulations of the riding profile for each of the investigated drive configurations in the time-domain by a more general method, similar to what is done in the design of electrical machines for EV and HEV for evaluation and comparison between different machine designs or machine types [14], [15] or [16].

Operating area analysis provides such a tool, and we distinguish two cases: With "steady-state operating area," we refer to (1), the requirement on the pairs of torque and speed the drive has to be able to produce. With "dynamic operating area," we denote (2), the requirement on the pairs of torque-slope and speed on the drive. As the analysis of the ability of a drive to produce a certain torque-speed pair is carried out, information on the drive efficiency for each operating point becomes easily available. From the values of the efficiency, three-dimensional efficiency-maps and two-dimensional efficiency-contour plots are obtained. The most important characteristics of the work presented here are that the analysis is based on data measured with real road tests and that both sides of the gear are included in the discussion.

IV. Riding Interval Profile Recordings

In this work, we determine the requirements on the operating areas from riding profiles obtained from real road tests. These profiles had been recorded with a commercially available bicycle that was equipped with a Power Tap® hub [17] to directly measure the torque and speed in the hub of the rear wheel of the test bicycle. The measurements were designed to obtain road data of "real-life applications." To this aim, riding interval profiles, profiles no. 1 through 4, of four different riders and with intervals of 15 to 25 minutes were recorded, where the bicycle was used for a short leisurely ride, grocery shopping, or commuting (Table I). The sampling interval was set to its minimum time, $t_s = 1.26$ s. These tests have been extensively reported on in [8].

TABLE I
Characteristics of Recorded Riding Profiles

Profile no.	Rider weight kg	Riding interval min	$P_{mech,max}$ W	$P_{mech,ave}$ W	T_{max} Nm	T_{ave} Nm
1	50	18	204.0	35.6	27.9	4.7
2	75	16	389.1	133.9	40.8	8.2
3	85	22	368.6	66.3	26.4	5.9
4	95	25	857.0	179.0	50.2	9.9

Riding profiles 1 and 4 illustrate the spread of the profile characteristics, and thus requirements on the drive, they are those with the lowest and highest torque and power demands respectively (It should be noted that the maximum speed of the riding profile 4 exceeds the speed limit for low-speed electric bicycles according to U.S. law, which is 20 mph.). The characteristics of riding profiles 2 and 3 are in-between these two extremes.

V. Steady-State Operating Area Requirements

A. Direct drives

The steady-state operating area requirements of the recorded riding profiles are displayed by a grid, where the torque is shown on the x-axis, and the wheel-speed on the y-axis. The grid dimensions are 1 Nm × 1 rad/s. The frequency of occurrence of the operating points enclosed in one grid element (in percent) is indicated by the color of the grid element. The steady-state operating area obtained from the compilation of all four rides together is shown in Fig. 1. With direct drives, the capability curves of the drive must include the required steady-state operating area.

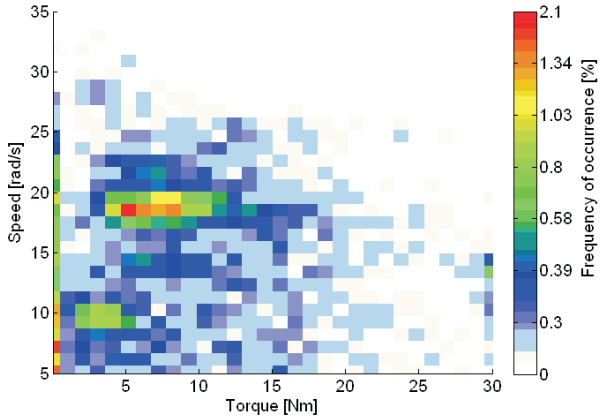

Fig. 1. Direct drive: steady-state operating area of all four riding profiles together. The colors indicate the frequency of occurrence of the operating points enclosed by the individual grid elements (in percent).

B. Geared drives

The main parameter for describing a drive with a gear is the gear ratio i, that correlates the input and output speeds ω_{in} and ω_{out} (here: mechanical speed of the motor shaft and bicycle wheel speed),

$$i = \frac{\omega_{in}}{\omega_{out}} \quad . \tag{1}$$

In the case of an ideal gear, it is also

$$i = \frac{T_{out}}{T_{in}} \quad , \tag{2}$$

with the gear input and output torques T_{in} and T_{out}.

Exact calculation of the gear efficiency η_{gear} is difficult, since it depends on many factors such as tooth friction and bearing efficiency. However, a so-called "rest efficiency" can be used as approximation for first-cut gear design [18]:

$$\eta_{gear} = -\frac{1 - i \cdot (0.99)^2 \cdot 0.995}{i} \tag{3}$$

The gear efficiency η_{gear} can be considered in two ways: (i) inclusion of η_{gear} into the determination of the operating area requirements and comparison of these to the capability of the direct drive for a first selection of the drive, (ii) comparison of the operating area requirements as determined for an ideal

gear and inclusion of η_{gear} into the calculation of the efficiency of the drive including the gear in a post-processing step.

Both approaches can be justified. In the first step, we use approach (i) and include the η_{gear} into the determination of the requirements given by the riding profiles. We thereby focus on the requirements on the system "before the gear," comprising the motor, the inverter, and the controller, which can then be properly selected to fulfil these requirements. Exemplarily, the steady-state operating area of all four rides and with gear ratio $i = 10$ is shown in Fig. 2. Approach (ii) will be applied further down in Section VIII-B when the focus is shifted to the drive efficiency.

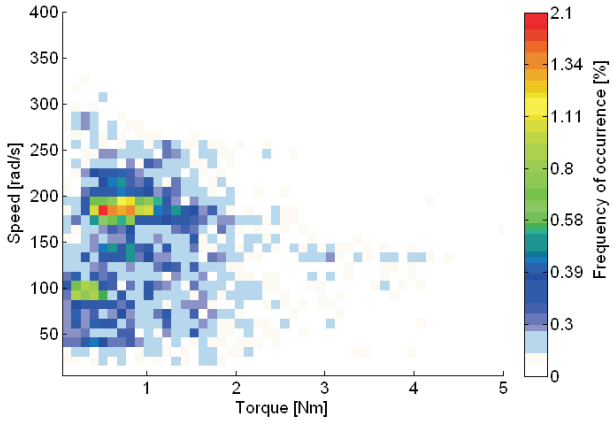

Fig. 2. Geared drive with $i = 10$, gear-efficiency according to (3): steady-state operating area of all four riding profiles together (values at motor shaft, compare with Fig. 1). The colors indicate the frequency of occurrence of the operating points enclosed by the individual grid elements (in percent).

VI. Dynamic Operating Area Requirements

A. Direct drives

The dynamic operating areas of the recorded riding profiles are displayed by a grid, where the torque-slope is shown on the x-axis, the wheel-speed on the y-axis, and the grid dimensions are 1 Nm/s $\times$ 1 rad/s. Again, the frequency of occurrence of the operating points enclosed in one grid element (in percent) is indicated by the color of the grid element. The results for $\frac{dT}{dt} = 0$ correspond to the steady-state case. The dynamic operating area obtained from the compilation of all four rides together is shown in Fig. 3.

B. Geared drives

In analogy to the steady-state case, the dynamic operating area for geared drives is derived from the requirements for direct drives and using the gear ratio i. Exemplarily, the dynamic operating area of all four rides and with gear ratio $i = 10$ is shown in Fig. 4.

VII. Model Implementation

A. Overview

The operating areas given drives can produce, as well as the efficiencies at the different operating points, are determined by

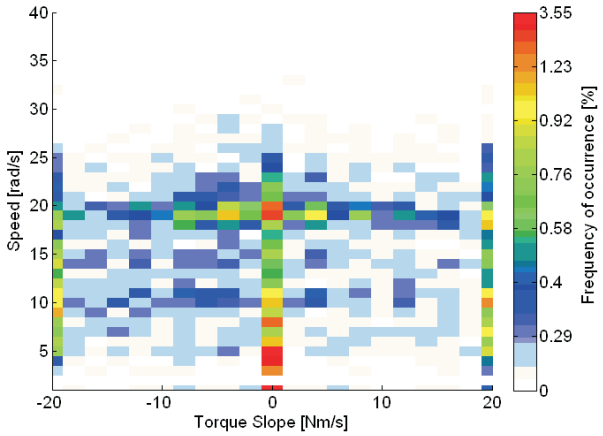

Fig. 3. Direct drive: dynamic operating area of all four riding profiles together. The colors indicate the frequency of occurrence of the operating points enclosed by the individual grid elements (in percent).

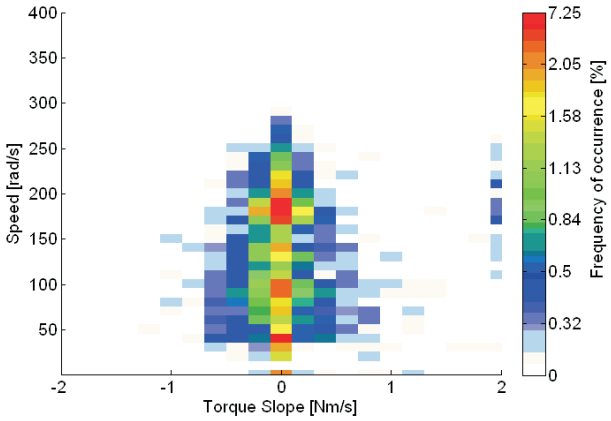

Fig. 4. Geared drive with $i = 10$, gear-efficiency according to (3): dynamic operating area of all four riding profiles together (values at motor shaft, compare with Fig. 3). The colors indicate the frequency of occurrence of the operating points enclosed by the individual grid elements (in percent).

means of a model that has been implemented using the commercially available software package MATLAB® Simulink® and a module-based approach. The three sub-modules, that each consist of further sub-modules, are the motor, the inverter, and the controller module. These have been described more extensively in [9], but in a different context, and are only briefly reviewed here. The influence of the gear ratio is considered either (i) in the variation of the requirements (Sections V-B and VI-B) or (ii) in a post-processing step (Section VIII-B) . As we only seek to determine if a motor can produce a given pair of (1) torque and speed, and (2) torque-slope and speed, this model does not include the mechanical equation, but the speed and torque are inputs to the model. The performances of the drives at the different individual operating points are determined by sweeping the ranges of the command T_{cmd} torque and shaft speed ω_{m} over the range of interest (Fig. 5).

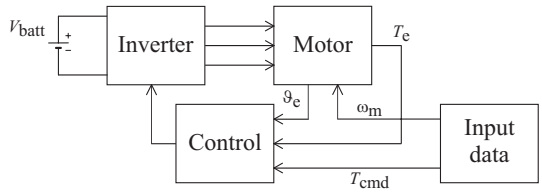

Fig. 5. Model of the drive system, data to sweep the operating area are used as input.

B. Motor module

We use the commercially available BLDC-motor model that is included in the PLECS®-Package of Plexim GmbH [19] as core of the motor module. If used as provided, the model includes the mechanical equation that relates the torque differential at the shaft and the acceleration. It has the load torque acting on the shaft as input parameter and the motor speed is calculated from the load torque and the mechanical equation. It is then used as input parameter for the calculation of the back EMF and of the rotor position. However, in this work, the motor speed is used as input parameters and the mechanical equation in the bicycle model is bypassed. Thereby, any inaccuracies possibly introduced by the simplified modeling of the system through the mechanical equations and the values of the associated parameters are avoided. With respect to the loss calculation, this certainly introduces an inaccuracy, notably for higher speed. We accept this compromise to avoid too many parameters of influence and to focus on the feasibility and methodology of the approach.

C. Control strategies

Since we focus on the investigation of the methodology, so as not to distract from this objective, we don't include the well-known pulse-width modulation (PWM) control. Two different control strategies, self-control and hysteresisband control (direct torque control, DTC), are implemented for illustration. In the self-control (SC) mode, the inverter acts only as commutator. The motor current and therefore the electrical torque of the BLDC-motor are controlled by variation of the DC-voltage with a buck-converter [20]. The buck-converter for changing the dc-link voltage is a standard converter. With hysteresisband control, the current or torque is controlled directly. The feedback signal is compared to the reference signal in a comparator with a given amount of hysteresis and the driving transistor is turned off or on when the error exceeds the upper or falls below the lower limit of the hysteresisband [21]. As most of the commercially available motors for electric bicycles and pedelecs have a built-in torque sensor, we exploit the advantages of direct torque control and use this technique in the further analysis.

D. Inverter module

For both control strategies, self-control mode and hysteresis control (DTC), this module includes an ideal voltage source, a resistance, which represents the battery internal resistance, the dc-link capacitor, and the inverter. The inverter is build from six ideal MOSFETs which receive the switching signals from the controller module. For the self-control mode, it also includes a buck-converter consisting of an ideal MOSFET, a diode and an inductor. We limit our analysis to an ideal inverter, so as not to have too large variability and focus on the feasibility and methodology of the approach.

E. Controller module

For both control strategies, the flat area of the back-EMF is determined from the continuously increasing mechanical rotor angle. The controller determines the switching signals so that the current is in phase with the back-EMF flat area to obtain maximal torque and power. Furthermore, the switching signals are also used to control the current magnitude.

With respect to the hysteresisband control, the torque band was set to $\Delta T = 0.1\ T_{\mathrm{cmd}}$. This band was chosen to obtain a torque ripple comparable to the torque ripple seen with PWM and self-control (Note that the motor only sees the torque band converted with the gear ratio.).

In self-control mode, the duty cycle and therefore the output voltage of the buck-converter, which is the dc-link voltage of the inverter, is regulated by a PI-controller which operates on the torque error.

F. Efficiency calculations

The efficiency of the direct-drive $\tilde{\eta}$ is given by the ratio of (a) the power output of the battery and (b) the output power of the motor, where (a) is given by the product of the battery voltage and current, $V_{\mathrm{batt}} \cdot I_{\mathrm{batt}}$ and (b) by the product of electric torque and the motor speed, $T_{\mathrm{e}} \cdot \omega_{\mathrm{m}}$,

$$\tilde{\eta} = \frac{T_{\mathrm{e}} \cdot \omega_{\mathrm{m}}}{V_{\mathrm{batt}} \cdot I_{\mathrm{batt}}} \quad . \tag{4}$$

The efficiency of the geared drive $\bar{\eta}$ is determined in a post-processing step,

$$\bar{\eta} = \tilde{\eta} \cdot \eta_{\mathrm{gear}} \quad , \tag{5}$$

using the gear efficiency η_{gear} as given by (3).

G. Motor parameter selection

Two different 24V motors are selected for the analysis (Table II):

1) A "high-torque motor" [23] which has output parameters comparable to commercially available bicycle motors.
2) A "high-speed motor" [24] that has only approximately one third of the torque of the high-torque motor but approximately 2.2 times higher speed.

VIII. Steady-State Operating Area

A. Direct Drives

We first determine the steady-state operating areas for the direct drives without gears using the approach described above (Section VII, Fig. 5). The command torque is varied from $0\ \mathrm{Nm} \leq T_{\mathrm{cmd}} \leq 5.0\ \mathrm{Nm}$ with a step-size of $\Delta T_{\mathrm{cmd}} = 0.1\ \mathrm{Nm}$. The speed feedback is varied from $0\ \mathrm{rad/s} \leq \omega_{\mathrm{m}} \leq 400\ \mathrm{rad/s}$

TABLE II

PARAMETERS OF THE MOTORS USED IN THE SIMULATIONS

		high-speed motor	high-torque motor
Peak torque	[Nm]	2.3	7.6
Rated torque	[Nm]	0.42	1.33
Rated speed	[rpm]	7400	3300
Rated power	[W]	328	459
Back-EMF constant	[V/rad/s]	0.0148	0.0325
Stator resistance	[Ω]	0.0345	0.0345
Stator inductance	[mH]	0.0645	0.1
Input voltage	[V]	24	24
Rated current	[A]	16.4	23
Friction torque	[Nm]	$7.5{\cdot}10^{-4}$	$7.5{\cdot}10^{-4}$
Rotor inertia	[Nm/s^2]	$42.3{\cdot}10^{-6}$	$12.7{\cdot}10^{-6}$
No. of poles		8	8

with a step-size of $\Delta\omega_{\mathrm{m}} = 10$ rad/s in the inner loop. For every step, the command torque and the speed feedback are held constant until the machine reaches the steady-state value. Then, the efficiency and electric torque at the commanded torque-speed pair are recorded. For the high-torque motor, the analysis is carried out both for self-control mode and for hysteresisband control. For the high-speed motor, only hysteresisband control is investigated.

The efficiency-maps are displayed as three-dimensional plots. When the drive cannot deliver the command torque within a certain tolerance-band ΔT_{e}, $|T_{\mathrm{cmd}} - T_{\mathrm{e}}| > \Delta T_{\mathrm{e}}$, the efficiency of this operating point is set to zero. Here, it is $\Delta T_{\mathrm{e}} = 0.1\ T_{\mathrm{cmd}}$. The interim values between the grid determined by the step-size are interpolated with the MATLAB® interpolation function included in the "mesh" command. Exemplarily, the efficiency-map of the high-torque motor with hysteresisband control is shown in Fig. 6.

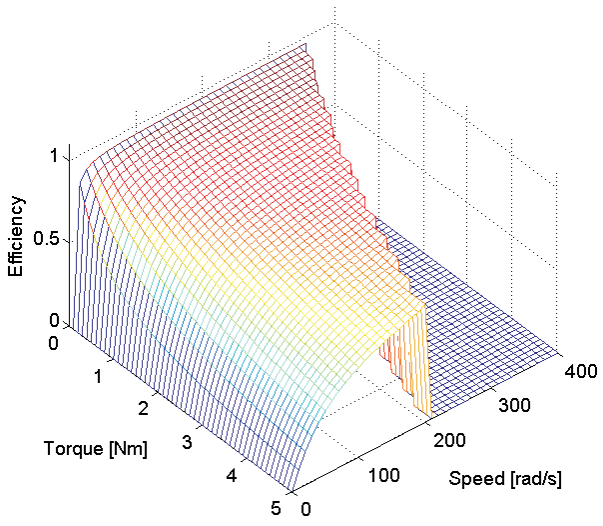

Fig. 6. Direct drive, hysteresisband control: efficiency-map of the high-torque motor.

For better comparison of the results for different control strategies, efficiency-contours can be plotted, where the operating points with "zero efficiency" are removed. Exemplarily, the results of the high-torque motor with hysteresisband control are shown in Fig. 7, corresponding to the efficiency-map shown in Fig. 6.

For both control modes, the drive efficiency is higher in the low-torque high-speed area, confirming the increased drive efficiency at larger gear ratios. This result will even be stronger as the gear efficiency increases with the gear ratio (Section VIII-B). At the same time, it has to be noted (a) that neither core nor inverter switching losses have been included in these calculations and (b) that a trade-off with the increase in size will have to be made.

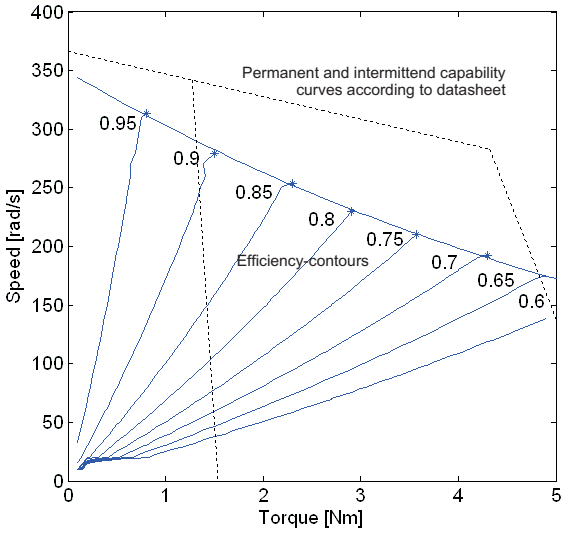

Fig. 7. Direct drive, hysteresisband control: efficiency-contours of the high-torque motor (compare with Fig. 6).

The capability curves, which are the envelopes of the operating area, are obtained from the endpoints of the efficiency-contours. They are given by the maximum torque that the drive can produce for the different speed. The capability curves are approximated with an exponential function of the form $\omega_{\mathrm{max}}(T_{\mathrm{e}}) = A \cdot e^{-\lambda T_{\mathrm{e}}}$. The parameters A and λ are determined to reach the minimum error between the fitted curve and the capability curves using unconstrained linear optimization. (We use the "fminsearch" function of the MATLAB® curve-fitting toolbox.) At steady-state, the capability curves are almost the same for self-control and hysteresisband control (HB-motor), and the difference between the two motors is clearly to see (Fig. 8):

$$\omega_{\mathrm{max}}(T_{\mathrm{e}})_{\mathrm{HT,SC}} = 354.17 \cdot e^{-0.146 T_{\mathrm{e}}} \quad (6)$$

$$\omega_{\mathrm{max}}(T_{\mathrm{e}})_{\mathrm{HT,HB}} = 355.32 \cdot e^{-0.130 T_{\mathrm{e}}} \quad (7)$$

$$\omega_{\mathrm{max}}(T_{\mathrm{e}})_{\mathrm{HS,HB}} = 779.27 \cdot e^{-0.3322 T_{\mathrm{e}}} \quad (8)$$

The difference between (i) the capability curves for the motor only, as given on the data-sheet, and (ii) those for the drive as determined by the simulation, increases with increasing torque: The larger current to obtain the larger torque leads to a higher voltage drop at the resistances and the machine inductance during commutation.

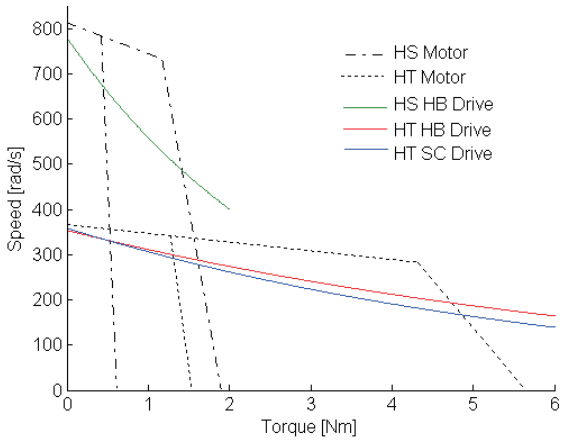

Fig. 8. Direct drive, self-control mode and hysteresisband control: steady-state capability curves $\omega_{\max}(T_e)_{HT,SC}$ and $\omega_{\max}(T_e)_{HT,HB}$ of the high-torque motor and $\omega_{\max}(T_e)_{HS,HB}$ of the high-speed motor ($\omega_{\max}(T_e)_{HT,SC}$, $\omega_{\max}(T_e)_{HT,HB}$, and $\omega_{\max}(T_e)_{HS,HB}$ according to (6)–(8)).

B. Geared Drives

The capability curves (Fig. 8) are compared to the operating area requirements (Section V, Fig. 2): With the gear ratio reduced to $i = 10$, the motor operating area required by the riding profile can be nearly completely covered by the drive. However, with the relatively high torque requirements, the motor more frequently works in the intermittent operation area. For example with a gear ratio $i = 22$, a larger part of the required operating area lies outside of the operating area of the drives. However, most of those operating points that the drive can produce are within the area of continuous operation of the motor.

In this part of the analysis, in addition to identifying wether a drive is able to produce a given torque-speed profile or not, we are also interested in the efficiency of the complete drive, including the gear. We therefore include the gear efficiency into the calculation of the efficiency-map and efficiency-contours of the drive according to (5). Exemplarily, the results of the high-torque motor with hysteresisband control and for gear ratios i = 10 and i = 22 are shown in Fig. 9. When comparing Figs. 7 and 9(a), the decrease of the efficiency of the overall drive due to the gear becomes obvious.

IX. Dynamic Operating Area

A. Direct Drives

Drawing from the results above (Section VI), we determine the requirements on the dynamic operating area of the drives to be the ranges of the torque slope $-20\ \frac{\text{Nm}}{\text{s}} \leq \frac{T_{\text{cmd}}}{dt} \leq 20\ \frac{\text{Nm}}{\text{s}}$ and of the bicycle wheel speed 0 rad/s $\leq \omega_{\text{m}} \leq 30$ rad/s. As the analysis of the operating area at steady-state showed that the selected motors are not suitable for use as direct drives in this context, we directly move on and only analyze the dynamic riding profiles for geared drives.

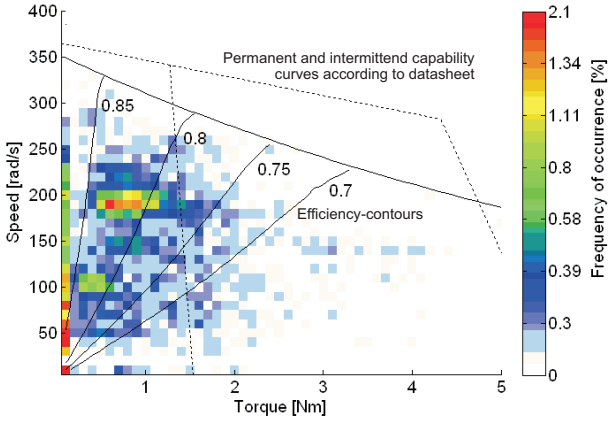

(a) Gear ratio $i = 10$.

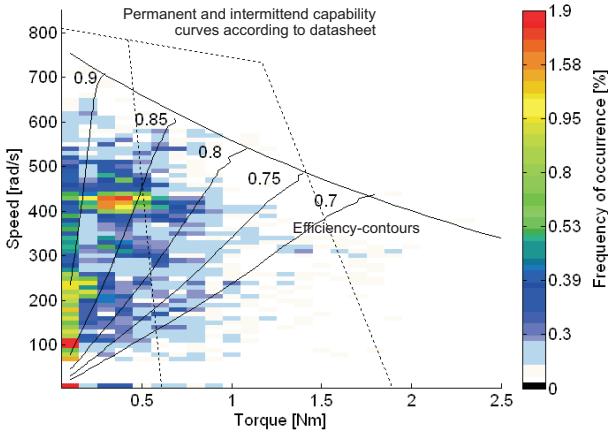

(b) Gear ratio $i = 22$.

Fig. 9. Geared drive, hysteresisband control: efficiency-contours of the high-torque motor with two different gear ratios compared to the required steady-state operating area of all four riding profiles together. The colors indicate the frequency of occurrence of the operating points enclosed by the individual grid elements (in percent).

B. Geared Drives

With a minimum gear ratio of $i = 10$ the range of the command torque slope is reduced down to $-2\ \frac{\text{Nm}}{\text{s}} \leq \frac{T_{\text{cmd}}}{dt} \leq 2\ \frac{\text{Nm}}{\text{s}}$. For the simulation, a step-size of $\Delta\frac{T}{dt} = 0.2\ \frac{\text{Nm}}{\text{s}}$ is selected. The speed feedback is varied from 0 rad/s $\leq \omega_{\text{m}} \leq 400$ rad/s with a step-size of $\Delta\omega_{\text{m}} = 10$ rad/s in the inner loop. The analysis is again carried out for self-control mode and for hysteresisband control.

For each operating point, the performance of the drive is evaluated by means of the artificially introduced parameter "TorqueError," T_{err}, which is derived from the command torque, T_{cmd}, and the electrical torque of the machine, T_{e}.

$$T_{\text{err}} = \frac{|T_{\text{cmd}} - T_{\text{e}}|}{T_{\text{cmd}}} \tag{9}$$

The results are displayed in a three-dimensional plot. The interim values between the grid determined by the step-size are again interpolated with the MATLAB® interpolation function

included in the "mesh" command. The values of T_{err} for self-control mode and hysteresisband control are shown in Figs. 10 and 11 respectively. For better comparison of the results, we also plot the T_{err} contour-plots (Figs. 12 and 13[1]).

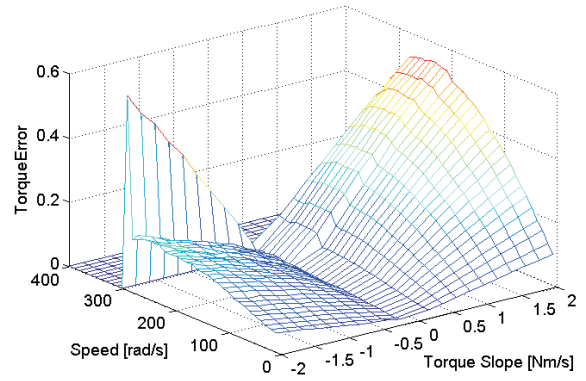

Fig. 10. Self-control mode: dynamic operating area of the high-torque motor.

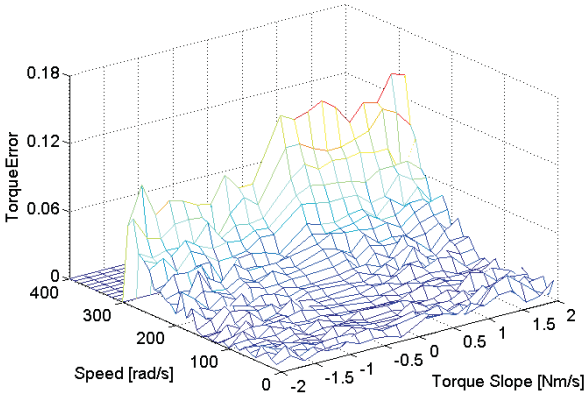

Fig. 11. Hysteresisband control: dynamic operating area of the high-torque motor.

Although both control strategies have very similar performances at steady-state, the difference in the dynamic case is very significant:

1) Self-control mode: T_{err} increases with higher torque slopes but does not increase for higher speeds. For the high-torque motor, T_{err} is larger than 20% for higher torque slopes ($\approx$ above 1 Nm/s) and operating speeds above 150 rad/s. For torque slopes in the range $-0.3\ \frac{\text{Nm}}{\text{s}} \leq \frac{T_{\text{m}}}{dt} \leq 0.1\ \frac{\text{Nm}}{\text{s}}$ T_{err} is smaller than 5% over the whole investigated speed range. The asymmetry of the results relative to the imaginative zero point is due to the PI-controller configuration of the buck-converter.

2) Hysteresisband control: T_{err} is almost constant over the whole investigated slope range, but increases with increasing speed, even for small torque slopes. For example, again for the high-torque motor, T_{err} is approximately constantly less than 5% up to 150 rad/s and larger than 8% above 250 rad/s, in both cases over the whole investigated range of the torque slope.

[1]Step-size of $\Delta\omega_{\text{m}} = 25$ rad/s in the inner loop.

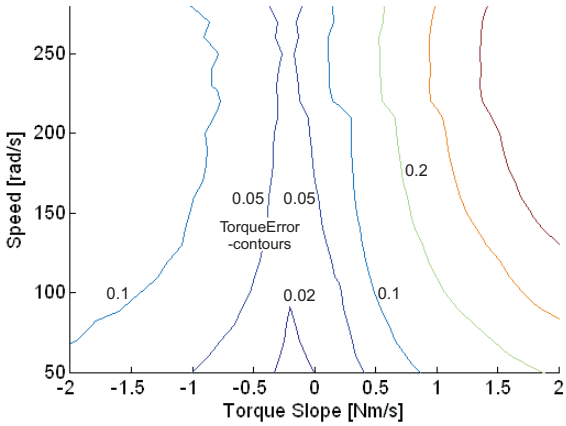

Fig. 12. Self-control mode: TorqueError-contours of the dynamic operating area of the high-torque motor.

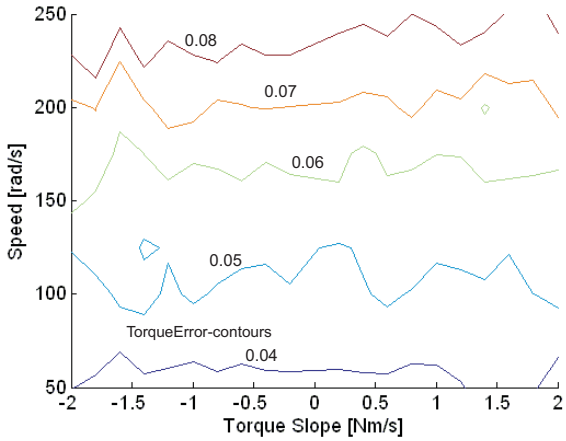

Fig. 13. Hysteresisband control: TorqueError-contours of the dynamic operating area of the high-torque motor.[1]

These results illustrate that one or the other control technique has to be preferred for applications with high demands on the torque or on the torque slope. Unfortunately, many riding profiles with high requirements on the torque also require high torque slopes so that a trade-off will have to be made. At the same time, the combination of steady-state and dynamic area analysis as shown is a suitable tool to design such drives and best identify the designs with the smallest compromise.

X. Conclusions

Different measured bicycle riding profiles were used to determine the steady-state and the dynamic operating area requirements of electric bicycles. The results illustrate the spread of the requirements but also the significance of considering the frequency of occurrence of the different operating points. Using these data as a starting point, techniques to investigate the technical performance of direct and of geared brushless-dc motor drives for such applications, including efficiency-maps and -contours were discussed. These include two different ways to consider the gear. The analysis shows the large

influence of the control-method on the drive operating area and the reduction of the drive operating area but at a higher drive efficiency with higher gear ratios. Furthermore, the operating areas of the drive in self-control mode and with hysteresisband control are almost equal in the steady-state case but very different in the dynamic case. While the self-mode control is rather constant over a wide speed range, hysteresisband control is rather constant with varying torque slope. Inverter loss and motor core loss, as well as the common full PWM control technique were not included in the analysis as the focus was laid on the investigation of the methodology as such, notably with respect to the consideration of the gear. In general terms, the self-control mode with higher gear ratio allows drive operation in more efficient operating areas, but the higher speed also causes the limitation of the drive operation area. Furthermore, a reduced gear ratio and therefore a reduced maximal torque reduces the dynamic operating area of the motor, since the maximum achievable torque slope decreases. At the same time, the steady-state operating area is hardly reduced, because even with a gear ratio of $i = 10$ the torque hardly limits the operation area of the motor. The reduced maximum torque slope will cause a lower bicycle acceleration but increase the maximal speed limit.

APPENDIX

Appendix A: List of abbreviations

Acronym	Definition
DC	Direct Current
BLDC	Brushless DC
DTC	Direct Torque Control
EMF	Electromagnetic Force
HB	Hysteresisband
PWM	Pulse-Width Modulation
SC	Self-control

Appendix B: List of symbols

Name	Description
i	gear ratio
T_{cmd}	command torque
T_{e}	electric torque
T_{err}	torque error (dynamic operating area)
T_{in}	input torque (gear)
T_{out}	output torque (gear)
V_{batt}	battery voltage
ϑ_{e}	rotor angle (electric degrees)
η_{gear}	gear efficiency
$\tilde{\eta}$	drive efficiency with ideal gear
$\bar{\eta}$	drive efficiency with non-ideal gear
ω_{in}	input speed (gear)
ω_{m}	motor speed (shaft speed)
ω_{out}	output speed (gear)

REFERENCES

[1] B. Kumar and H. Oman, "Power control for battery-electric bicycles," *Proceedings of NAECON '93 - National Aerospace and Electronics Conference*, vol. 1, pp. 428-434, Dayton, OH, May 24-28, 1993.

[2] W.C. Morchin, "Battery-powered electric bicycles," *Proceedings of Northcon '94*, pp. 269-274, Seattle, WA, October 11-13, 1994.

[3] E.A. Lomonova, A.J.A. Vandenput, J. Rubacek, B. d'Herripon, and G. Roovers, "Development of an improved electrically assisted bicycle," *Proceedings of 37th IEEE IAS Annual Meeting*, pp. 384-389, Pittsburgh, PA, October 13-18, 2002.

[4] F.E. Jamerson, *Electric bikes worldwide 2002: with electric scooters & neighborhood EVs*, Naples, Fla: Electric Battery Bicycle Co, 2002.

[5] A. Muetze, A.G. Jack, and B.C. Mecrow, "Brushless-dc motor using soft magnetic composites as a direct drive in an electric bicycle," *Proceedings of the 9th European Conference on Power Electronics and Applications (EPE), paper no. 350, Graz, 2001.*

[6] D.G. Wilson, J. Papadopoulos, and F.R. Whitt, *Bicycling science*, Cambridge, Mass: MIT Press, 2004.

[7] P. Fairley, "China's cyclists take charge: electric bicycles are selling by the millions despite efforts to ban them," *IEEE Sprectrum*, vol. 42, no. 6, pp. 54-69, June 2005.

[8] A. Muetze and Y.C. Tan, "Performance evaluation of electric bicylces," *Proceedings of 40th IEEE IAS Annual Meeting*, pp. 2865-2872, Hong Kong, October 2-6, 2005; to appear in IEEE Industry Applications Magazine (July 2007).

[9] E. Starschich and A. Muetze, "Comparison of the performances of different geared brushless-dc motor drives for electric bicycles," *Proceedings of the IEEE 5th International Electric Machines and Drives Conference (IEMDC 2007)*, pp. 140-147, Antalya, Turkey, May 2-5, 2007.

[10] SANYO Electric Co., Ltd., "SANYO – SANYO Electric Co., Ltd.," leaflet, available at http://www.jbpi.or.jp/english/jbg.html, accessed October 14, 2006.

[11] Panasonic Cycle Technology Co., Ltd., http://www.panabyc.co.jp/en/product_du.htm, accessed October 14, 2006.

[12] Sachs, "Sachs-Bikes: E-Bikes," http://www.sachs-bikes.de/produkte.php? marken_id=1&prod_cat=5, accessed October 14 2006.

[13] NewRide, "Fahrzeugkatalog 2006," available at http://www.newride.ch, accessed October 14, 2006.

[14] S. Williamson, S. Lukic, and A. Emadi, "Comprehensive drive train efficiency analysis of hybrid electric and fuel cell vehicles based on motor-controller efficiency modeling," *IEEE Transactions on Power Electronics*, vol. 21, no. 3, pp. 730–740, May 2006.

[15] G. Pugsley, C. Chillet, A. Fonseca, and A-L. Bui-Van, "New modeling methodology for induction machine efficiency mapping for hybrid vehicles," *Proceedings of 4th IEEE Electric Machines and Drives Conference (IEMDC '03)*, vol. 2, pp. 776-781, Madison, WI, June 1–4, 2003.

[16] J.P. Altendorf, T. Baumann, C.E. Carstensen, R.B. Inderka, and A. Lange, "Assessment criteria for electrical drives in electric-, hybrid- and fuel cell vehicles within the OKOFEH-project," *20th International Electric Vehicle Symposium (EVS-20)*, Long Beach, USA, November 15–19, 2003.

[17] Power Tap® is by Graber Products, Inc., 5253 Verona Road, Madison, WI USA, http://www.cycle-ops.com.

[18] VDI, *VDI-Richtlinie: VDI 2157 Planetengetriebe; Begriffe, Symbole, Berechnungsgrundlagen* [VDI-Guideline: VDI 2157 Planetary gears; terms, symbols, calculation], 1978.

[19] Plexim GmbH, http://www.plexim.com, accessed October 14, 2006.

[20] B.K. Bose, *Modern Power Electronics and AC Drives*, Prentice Hall, 2002.

[21] J.R. Hendershot and T. Miller, *Design of brushless permanent-magnet motors*, 1994.

[22] Moog Components Group, "Silencer Series Brushless DC Motors Commercial and Industrial," http://www.polysci.com/Motors/silencer.html, accessed October 14, 2006.

[23] Moog Components Group, motor BN34-45AF-01, in [22].

[24] Moog Components Group, motor BN34-25AF-01, in [22].